these radiation-dependent features could distinguish irradiated tumor better than human eye.

Material and Methods: Rhabdomyosarcoma R1 tumors grown on the lateral flank of WAG/Rij rats were irradiated with 12 Gy or 0 Gy (control). Computed tomography (CT) scans were acquired both before and 7 days post RT [2]. These data were used as a training dataset to select RT-related features. For validation, radiomics features were extracted from CT images of head and neck squamous cell carcinoma (HNSCC) patients before and post 10 fractions of radiation. A total of 723 features were extracted and the top 100 robust features were selected for further analysis based on inter-class correlation coefficient (ICC) values obtained from test-retest (TRT) scans. Imaging experts and radiation oncologists were consigned to identify irradiated tumors (IR) vs. non-irradiated (Non-IR) tumors blinded for patient information. Area under the curve of the receiver operating characteristics curve (AUC-ROC) was computed for each individual feature identified in the rat and HNSCC datasets as being both stable and significant for distinguishing IR and non-IR tumors.

Results: 17 significant differentially expressed features were identified between the two imaging time points after TRT feature selection. 8 out of 17 (2 shape and 6 wavelets) significantly ($p<0.05$) distinguished between pre and post RT scans. AUC-ROC curves demonstrate that out of 8 features, 2 shape and 4 wavelet features had an accuracy of 0.71 and >0.62 respectively in identifying IR tumor from the non-IR ones, whereas imaging experts could only correctly identify 56% (56 ± 5.7) of true cases in rats. 2 (shape) out of 8 features identified in rats also were found to be significantly different between pre and post RT in HNSCC patients (Fig. 1). These two features had an AUC-ROC of 0.85 in identifying a IR tumor while, radiation oncologists were able to solely identify 50% (50 ± 5.6) of true cases in HNSCC patients.

Conclusion: RT radiomics features identified in rats and HNSCC patients were able to distinguish irradiated tumors better than human eye. Thus, in future these features might be used for dosimetric measures and might help in segregating effects of RT from combination treatments that enables to understand the effect of drug or RT alone.

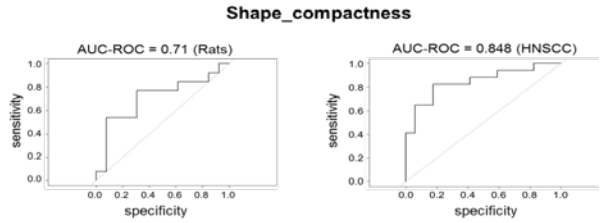

OC-0071

Analysis and reporting patterns of failure in the era of IMRT: head and neck cancer applications

A.S.R. Mohamed[1], D.I. Rosenthal[1], M.J. Awan[2], A.S. Garden[1], E. Kocak-Uzel[3], A.M. Belal[4], A.G. El-Gowily[5], J. Phan[1], B.M. Beadle[1], G.B. Gunn[1], C.D. Fuller[1]

[1]*MD Anderson Cancer Center, Radiation Oncology, Houston, USA*

[2]*Case Western University, Radiation Oncology, Cleveland, USA*

[3]*Şişli Etfal Teaching and Research Hospital, Radiation Oncology, Istanbul, Turkey*

[4]*Alexandria University, Radiation Oncology, Alexanria, Egypt*

[5]*Alexandria University, radiation Oncology, Alexandria, Egypt*

Purpose or Objective: To develop a methodology to standardize the analysis and reporting of the patterns of loco-regional failure after IMRT of head and neck cancer.

Material and Methods: Patients with evidence of local and/or regional failure following IMRT for head-and-neck cancer at MD Anderson cancer center were retrospectively reviewed under approved IRB protocol. Manually delineated recurrent gross disease (rGTV) on the diagnostic CT documenting recurrence (rCT) was co-registered with the original planning CT (pCT) using both deformable (DIR) and rigid (RIR) image registration software. Subsequently, mapped rGTVs were compared relative to original planning target volumes (TVs) and dose using volume overlap and centroid-based approaches. Failures were then classified into five types based on combined spatial and dosimetric criteria; A (central high dose), B (central elective dose), C (peripheral high dose), D (peripheral elective dose), and E (extraneous dose) as illustrated in figure 1.Paired-samples Wilcoxon signed rank test was used to compare analysis metrics for RIR versus DIR registration techniques.

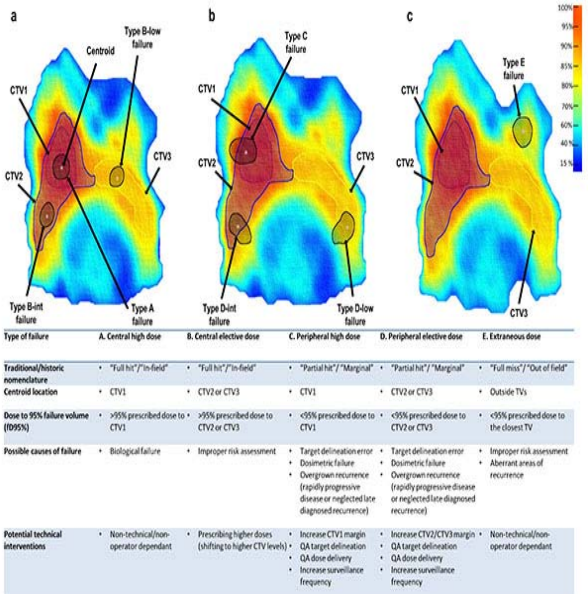

Results: A total of 21 patients were identified. Patient, disease, and treatment characteristics are summarized in table 1. The registration method independently affected the spatial location of mapped failures (n=26 lesions). Failures mapped using DIR were significantly assigned to more central TVs compared to failures mapped using RIR for both the centroid-based and the volume overlap methods. 42% of centroids mapped using RIR were located peripheral to the same centroids mapped using DIR (p= 0.0002), and 46% of the rGTVs whole volumes mapped using RIR were located at a rather peripheral TVs compared to the same rGTVs mapped using DIR (p< 0.0001). rGTVs mapped using DIR had significantly higher mean doses when compared to rGTVs mapped rigidly (mean dose 70 vs. 69 Gy, p = 0.03). According to the proposed classification 22 out of 26 failures were of type A as assessed by DIR method compared to 18 out of 26 for the RIR because of the tendencey of RIR to assign failures more peripherally.

Table 1. Patient demographics, disease, and treatment characteristics

	Total	
	n=21	(%)
Age (years)		
Median	58	
Range	30-75	
Time to Failure (months)		
Median	12	
Range	5-69	
Sex		
Male	18	(86)
Female	3	(14)
Origin		
Nasopharynx	6	(28)
Oropharynx	5	(24)
Hypopharynx	5	(24)
Unknown primary	5	(24)
T-category		
T0	5	(24)
T1	1	(5)
T2	7	(33)
T3	5	(24)
T4	3	(14)
N-category		
N0	1	(5)
N1	5	(24)
N2	12	(57)
N3	3	(14)
Treatment		
Radiation alone	4	(19)
Concurrent ChemoRadiation	9	(43)
Induction Chemotherapy + Radiation	1	(5)
Induction Chemotherapy + Concurrent ChemoRadiation	7	(33)
Radiation dose		
Mean (SD)	69.2	(1.7)
Radiation fractions		
Mean (SD)	33	(2)

Conclusion: DIR-based registration methods showed that the vast majority of failures originated in the high dose target volumes and received full prescribed doses suggesting biological rather than technology-related causes of failure. Validated DIR-based registration is recommended for accurate failure characterization and a novel typology-indicative taxonomy is recommended for failure reporting in the IMRT era.

OC-0072

Respiratory time-resolved 4D MR imaging for RT applications with acquisition times below one minute

C.M. Rank[1], T. Heußer[1], A. Wetscherek[1], A. Pfaffenberger[2], M. Kachelrieß[1]

[1]*German Cancer Research Center DKFZ, Medical Physics in Radiology, Heidelberg, Germany*

[2]*German Cancer Research Center DKFZ, Medical Physics in Radiation Oncology, Heidelberg, Germany*

Purpose or Objective: 4D MRI has been proposed to improve respiratory motion estimation in radiotherapy (RT), aiming to achieve a higher treatment accuracy in the thorax and the upper abdomen. In contrast to 4D CT, acquisition time in 4D MRI is not limited by radiation dose, such that multiple breathing cycles can be imaged routinely. However, standard MR reconstruction methods, such as gated gridding, have limitations in either temporal or spatial resolution, signal-to-noise ratio (SNR), contrast-to-noise ratio (CNR) and artifact level or demand inappropriately long acquisition times. The purpose of this study is to provide high quality 4D MR images from super short acquisitions.

Material and Methods: MR data covering the thorax and upper abdomen of three free-breathing volunteers were acquired at a 1.5 T Siemens Aera system. We applied a gradient echo sequence with radial stack-of-stars sampling and golden angle radial spacing: total acquisition time: 37 s, slice orientation: coronal, field-of-view: 400×400×192 mm^3, voxel size: 1.6×1.6×4.0 mm^3, TR/TE = 2.48/1.23 ms, 240 spokes per slice, undersampling factor: 16.8, flip angle: 12°. MR data were sorted into 20 overlapping 10% wide motion phase bins employing intrinsic MR gating. Respiratory motion compensated (MoCo) 4D MR images were generated using our newly developed 4D joint MoCo-HDTV algorithm, which alternates between motion estimation and image reconstruction. With MoCo, each motion phase is reconstructed from 100% of the measured rawdata. In the motion estimation step, the motion vector fields (MVFs) are estimated between adjacent motion phases and regularized by cyclic constraints. Results were compared to the standard reconstruction methods 3D gridding and 4D gated gridding.

Results: 3D gridding reconstructions revealed strong blurring of structures in the lungs, in the diaphragm region and in the liver caused by respiratory motion. 4D gated gridding images were deteriorated by noise and severe streak artifacts, arising from high azimuthal undersampling. These artifacts obscured small anatomical structures. In contrast, 4D joint MoCo-HDTV reconstructions yielded appropriate image quality combining low streak artifact levels and high temporal resolution, SNR, CNR and image sharpness. Thus, the displacement between end-exhale and end-inhale of small liver structures could be determined, which was not possible using 4D gated gridding images due to their limited image quality.

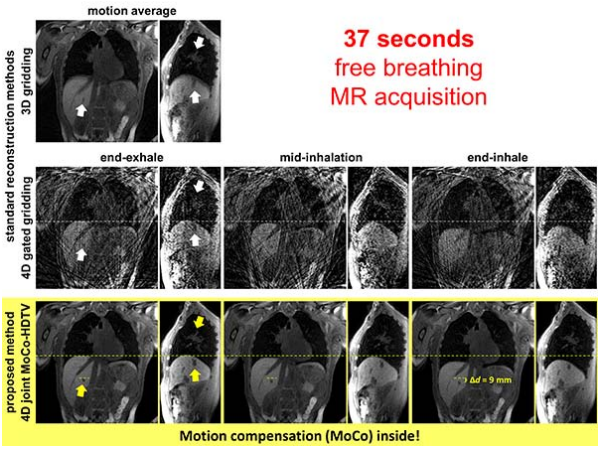

Conclusion: 4D joint MoCo-HDTV facilitates 4D respiratory time-resolved MRI and provides respiratory MVFs at acquisition times below one minute. The method is promising for reliable target delineation in radiation therapy, patient-specific margin or gating window definition, and for adaptive planning based on the provided MVFs. The short acquisition time makes it attractive also for online imaging in an MR-LINAC setting.

Proffered Papers: Physics 2: Basic dosimetry

OC-0073

Difference in using the TRS-398 code of practice and TG-51 dosimetry protocol for FFF beams

J. Lye[1], D.J. Butler[2], C.P. Oliver[2], A. Alves[1], I.W. Williams[1]

[1]*Australian Radiation Protection and Nuclear Safety Agency, Australian Clinical Dosimetry Service, Melbourne- Victoria, Australia*

[2]*Australian Radiation Protection and Nuclear Safety Agency, Radiotherapy, Melbourne- Victoria, Australia*

Purpose or Objective: The two most commonly used protocols for reference dosimetry in external beam radiotherapy are IAEA TRS-398 and AAPM TG-51. Increasingly flattening filter free (FFF) linacs are in clinical use and published theoretical analysis suggests that a difference of 0.5 % is expected between the two protocols (Xiong 2008).

Material and Methods: The Australian Clinical Dosimetry Service (ACDS) has measured FFF beam dose outputs on 11 linacs using both TRS-398 and TG-51 protocols. The response of an NE2561 chamber was modelled using DOSRZnrc. The model was used to study the difference in *kQ* in Varian and Elekta linacs when the flattening filter was removed, and when the flattening filter was replaced by a thin metal plate.

Results: Measured differences in dose output derived from TRS-398 and TG-51 protocols were less than 0.1 % for 6 MV FFF beams and less than 0.2 % for 10 MV FFF beams. Figure 1 shows the modelled response from the NE2561 for Elekta and Varian beams with the flattening filter, with the flattening filter removed, and with a thin metal plate replacing the flattening filter. The modelled FFF *kQ* as a function of TPR20,10 is 0.6 % lower than the *kQ* with flattening filter (WFF). This difference is reduced to 0.3 % when considering *kQ* as a function of %*dd*(10)x. Thus the measured difference in the TRS-398 and TG-51 protocols should be 0.3% according to the modelled results, however the average measured difference is less than 0.1 %. The commercial realisation of FFF beams includes a thin metal filter in the place of the flattening filter. When a 2-3 mm metal plate was included in the model, the difference between the FFF *kQ* and the WFF *kQ* was reduced to approximately 0.1%.